Biomedical Signal Processing and Control 14 (2014) 285–290

Contents lists available at ScienceDirect

Biomedical Signal Processing and Control

journal homepage: www.elsevier.com/locate/bspc

Computer modelling of beat-to-beat repolarization heterogeneity in human cardiac ventricles

György Kozmann[a], Gergely Tuboly[a,*], Vavrinec Szathmáry[b], Jana Švehlíková[c], Milan Tyšler[c]

[a] Department of Electrical Engineering and Information Systems, Faculty of Information Technology, University of Pannonia, Egyetem u. 10, Box 158, H-8201 Veszprém, Hungary
[b] Institute of Normal and Pathological Physiology, Slovak Academy of Sciences, Sienkiewiczova 1, 813 71 Bratislava, Slovakia
[c] Institute of Measurement Science, Slovak Academy of Sciences, Dúbravská cesta 9, 841 04 Bratislava, Slovakia

ARTICLE INFO

Article history:
Received 12 September 2013
Received in revised form 15 August 2014
Accepted 21 August 2014

Keywords:
QRST integral map
Non-dipolarity index
Numerical chest model
Numerical heart model

ABSTRACT

Based on our numerical heart and chest model with stochastically modifiable action potential duration (APD) parameters, the consequences of diminished subepicardial cell-to-cell coupling were studied on beat-to-beat repolarization heterogeneity. Pathological action potential durations and transmural gradient (TG) mean values (M) were assumed in the apical segment of the five-layer heart model, while in the rest of the model the action potential parameters were kept in the normal range. APD mean values and the associated APD standard deviations (SDs) were fitted to experimental data. SD was causally related to APD mean. Repolarization heterogeneity was characterized by QRST integral maps and by the non-dipolarity index (NDI). The TG of −15 model time units (mtu) yielded an NDI of 12%. By sweeping beat-to-beat TG from −15 mtu up to +14 mtu, NDI increased from 12% up to 71%. In healthy heart M is large compared to the SD value; consequently NDI is in the stable <20% range. In arrhythmia patients TG diminishes, M and SD increase, consequently, NDI shows temporally random, increased beat-to-beat fluctuations, suitable for the characterization of repolarization heterogeneity.

1. Introduction

Ventricular tachycardia (VT) and fibrillation (VF) are the most common causes of sudden cardiac death (SCD). In spite of the continuous development of risk assessment methods, still no reliable ECG based marker of arrhythmia prone status does exist according to the scientific statement of the AHA/ACCF/HRS based on hundreds of clinical trials [1].

According to theoretical expectations, parameters casually reflecting the spatial heterogeneity of the elementary myocardial volumes might be the clue of a more efficient risk assessment. Relying on sophisticated experimental observations, Abildskov et al. [2] suggested the use of body surface potential mapping for the characterization of malignant alterations of ventricular repolarization by QRST integral maps. The utility of QRST integral map-based repolarization disparity (RD) detection was proven theoretically by Plonsey [3] and Geselowitz [4]. As QRST integral maps are the surface projections of the ventricular heterogeneity distribution, the desired arrhythmia vulnerability sensitivity should be related to the pathological irregularities of the integral maps. Indeed, Hubley-Kozey et al. [5] proved statistically that a few uncorrelated spatial features of averaged QRST integral maps can identify the arrhythmogenic substrate in the myocardium. Karhunen–Loève (KL) expansion of QRST integral maps proved to be a valuable tool for diagnostic feature extraction. Even the single scalar non-dipolarity index (NDI) computed from KL coefficients could separate high-risk and low-risk population based on time-averaged QRST integral maps [6,7].

Other authors emphasized the utility of beat-to-beat repolarization lability measures [8,9] based on QT parameters (QT variability index) of conventional ECG leads. Within the most recent approaches it is worth mentioning the development of a simple but efficient arrhythmia vulnerability index, based on the averaged sum absolute QRST integrals (SAI QRST) of orthogonal-leads suggested by Tereshchenko et al. [10]. The definition of SAI QRST is related to the NDI, but for the simplicity of clinical measurements the information hidden in the "multipolar" source components is disregarded.

* Corresponding author. Tel.: +36 88 62 4224; fax: +36 88 62 4526.
E-mail addresses: kozmann.gyorgy@virt.uni-pannon.hu (G. Kozmann), tuboly.gergely@virt.uni-pannon.hu (G. Tuboly), Vavrinec.Szathmary@savba.sk (V. Szathmáry), umersveh@savba.sk (J. Švehlíková), umertysl@savba.sk (M. Tyšler).

http://dx.doi.org/10.1016/j.bspc.2014.08.008
1746-8094/

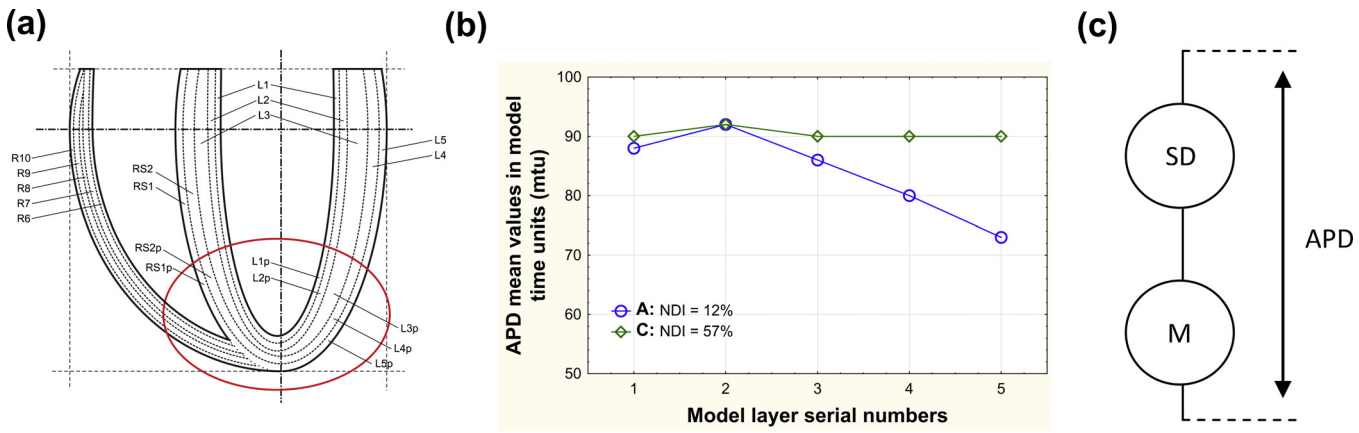

Fig. 1. (a) A schematic representation of the "layered" structure and geometry of the left and right ventricles. The ellipse at the apex contains the pathologically modulated area of the model. The labels of the layers can be interpreted as follows: initial capital letters 'L' and 'R' mark the left and right ventricles respectively, while 'RS' refers to the septum. The numbers represent the serial number of each layer. Small letters of 'p' at the end of the label indicate the pathological modulation of the model action potentials (MoAPs) related to the layer. (b) Mean value (M) of the APD profile of a healthy subject (profile A) and a failing heart patient (profile C) vs. the serial number of the model layers. The simplified graph is based on the experimental data of Glukhov et al. [12]. (c) Schematic representation of our APD model consisting of a constant component (M) and an additive Gaussian random component with standard deviation (SD).

The novelty in our approach published earlier was the use of beat-to-beat QRST integral map analysis instead of time-averaged QRST integral maps. This method allowed theoretically sound characterization of the stochastically changing spatio-temporal RD irregularities (lability) throughout a long train (typically 300) of cardiac cycles [11]. We could demonstrate that QRST integral maps, or even the extracted NDIs, computed from the KL coefficients of the QRST integral maps; characterize sensitively the spatio-temporal variability of the subsequent maps. According to our learning groups, NDI plots separated efficiently the group of implanted cardioverter (ICD) patients with documented malignant arrhythmia vulnerability from healthy subjects. In the arrhythmia group the beat-to-beat time series of the NDI values were uncorrelated and the corresponding NDI amplitude histograms showed skewed lognormal distributions, in certain cases with extreme NDI values going up to 90%. In healthy subjects the sequences of NDI values were correlated and the amplitudes remained typically in the range of (10%–20%) with slight quasi-periodic components, partly due to the respiration related positional heart changes.

In this study we attempted to link the observed normal and pathological QRST integral (and NDI) behaviour, to mesoscopic (intramural) and even to microscopic experimental findings. To this end, numerical chest and multi-element heart models were used. In the heart model, APD mean values of the different myocardial layers were approximated based on the recent optical mapping results of stained subepicardial, midmyocardial, and subendocardial sections taken from healthy and failing human hearts (Glukhov et al. [12]). The beat-to-beat APD variability estimates were taken from isolated cellular measurements of Zaniboni et al. and others [13,14]. Because in our previous study we demonstrated that the sources of measurable body surface QRST integral map variability are located mostly in the apical part of the heart, for the sake of modelling simplicity, the mesoscopic model action potential (MoAP) modulation was confined to the apical region [15].

2. Materials and methods

2.1. Numerical modelling of the heart

Details of the simplified computer model of the human cardiac ventricles were described previously by Szathmáry and Osvald [16]. The model was defined in a 3-dimensional matrix consisting of 1 mm^3 cubic elements. The local functional properties of the elementary volumes were represented by simplified model action potentials (MoAPs). The overall geometry of cardiac ventricles was defined analytically by segments of ellipsoids representing their inner (endocardial) and outer (epicardial) surfaces. The parameters of the ellipsoids were derived from the gross dimensions of the right and left ventricles (RV and LV), given as input data of the model. To simulate the fine structure of physiological repolarization heterogeneity, ventricular walls were sliced into 5 layers, paralleling with the inner and outer surfaces (Fig. 1(a)). The different fibre directions from the endo- to epicardial myocardium were not taken into account. The MoAP characteristics of model elements may be defined differently depending on their localization in respective layers.

In the reference model, simulating the normal activation, the gross dimensions of ventricles and the parameters of activation were derived from data published by Durrer et al. [17] and Hutchins et al. [18]. Ventricular depolarization was started from predetermined elements on the inner endocardial surface of both ventricles, corresponding to regions of earliest activation. The spread of activation in the most inner layer, representing the Purkinje mesh, was three times faster than in the remaining layers of the walls. After depolarizing of model elements their consecutive repolarization is governed by their action potential length and shape. The MoAP differences in respective layers cause a physiological transmural dispersion of cardiac action potential durations [19]. The activation and repolarization of the reference model, defined in this way correspond well to the generally accepted normal patterns of human heart activation.

The model allows a layer-by-layer modulation of ventricular wall AP parameters simultaneously in the whole ventricular myocardium or in a spatially limited region. An example is shown in Fig. 1(a), where the apical part (surrounded by the ellipse) has different APD profiles as it is shown in Fig. 1(b). In this study the apical segment of the myocardium has pathological APD profile [12]. In general, the geometry of local heterogeneities is always defined analytically by subsidiary ellipsoids.

The spread of the activation wave front is simulated by a cellular automaton. In each step of simulation the elementary dipole moments are computed as the potential differences between the adjacent cubic elements. Finally, the whole model of the cardiac ventricles' myocardium is divided into 33 volume segments. In each segment the dipole moments from all corresponding elements are summarized in its gravity centre, so finally a multiple-dipole equivalent cardiac generator is created.

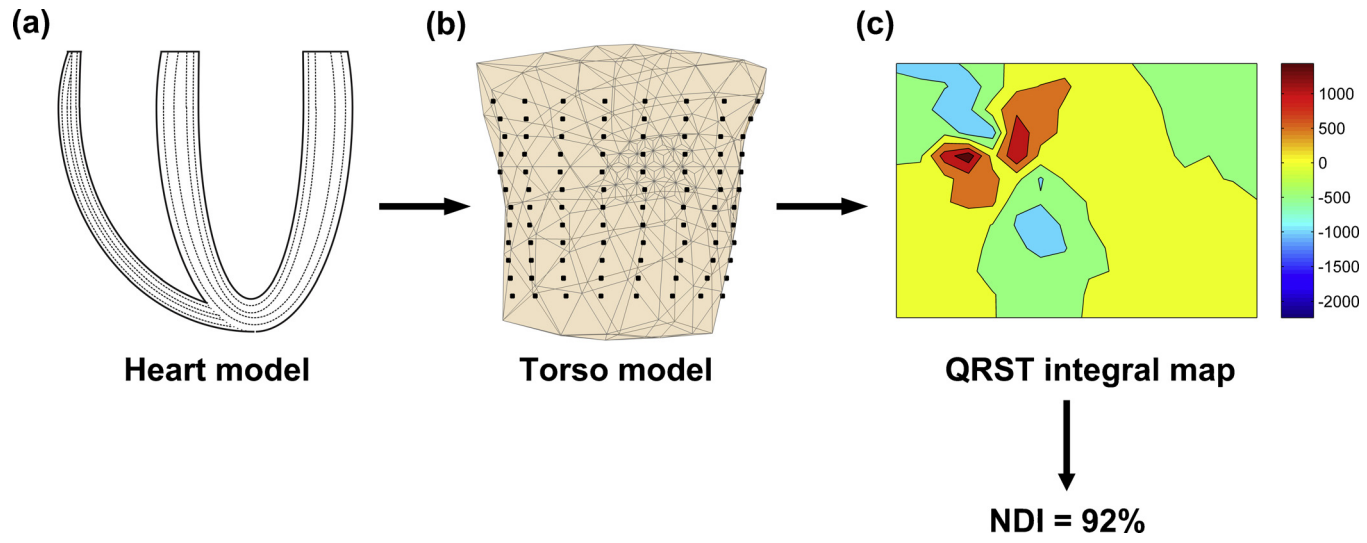

Fig. 2. Flow diagram of the simulation study. (a) Conceptual multi-layer programmable heart model (details are shown in Fig. 1). (b) Realistically shaped torso model with black points indicating the frontal position of nodes in regular mesh (192 points in total), in which the BSPM is computed. (c) QRST integral map and NDI computed from the generated data of the heart-thorax setup.

2.2. Modelling of the thorax, computation of body surface potential maps (BSPMs)

To compute the heart-generated potentials on the thoracic surface, the multiple-dipole cardiac generator is inserted in a realistically shaped piecewise homogeneous torso model (Fig. 2). Lungs are taken into consideration with 4× lower conductivity than general conductivity of the torso while ventricular cavities appear with 3× higher conductivity. Electric potentials on the body surface are computed in the surface points of the torso model using boundary element method (BEM), originally proposed by Barr et al. [20] and also used in current studies [21,22].

The use of BEM for computation of body surface potential maps $m(t)$ in Ne points on the body surface in each time instant t, yields a linear matrix equation:

$$m(t) = \mathbf{A}g(t) \tag{1}$$

where $\mathbf{A}$ is the time independent transfer matrix (i.e. the geometry and position of the heart and torso were fixed during the cardiac cycle), which represents the properties of the inhomogeneous torso as volume conductor and $g(t)$ is a multiple-dipole generator (with Ns current dipoles) in a particular time step of the heart activation. The integral BSPM p representing the integral of $m(t)$ over a particular time interval can then be described by Eq. (2).

$$p = \int m(t)dt = \int \mathbf{A}g(t)dt = \mathbf{A}\int g(t)dt = \mathbf{A}s \tag{2}$$

where s represents the time integrals of Ns dipole moments of modelled multiple dipole generator. Considering three orthogonal components of each dipole moment, the size of the transfer matrix $\mathbf{A}$ is $(Ne \times 3Ns)$.

The body surface potential maps are computed from the potentials in a regular mesh (12×16) on the body surface consisting of 192 points (Fig. 2(b)).

2.3. Evaluation of repolarization dispersion by QRST integrals and the non-dipolarity indices

According to Geselowitz, the amplitude of the QRST integrals at an arbitrary body surface point P is a function of the AP heterogeneity Eq. (3), in other words, it is the function of the gradient of the μ of MoAP areas of the myocardium [4]. Consequently, beat-to-beat application of Eq. (3) provides a non-invasive tool that can be used to study the spatio-temporal variability of AP properties i.e. the RD.

$$\int_{\mathrm{QRST}} \phi(P,t)dt = -k\iiint_{V_s} \mathbf{z}(P,\mathbf{r})\mathrm{grad}(\mu(\mathbf{r}))dV_s \tag{3}$$

where $\mu(\mathbf{r})$: area under the action potential, $\phi_m(\mathbf{r},t)$: membrane potential at time t, $\phi_{mr}(\mathbf{r})$: membrane resting potential at point $\mathbf{r}$, V_s: volume of sources (myocardium), k: constant, and z: vector of transfer coefficients between P and $\mathbf{r}$.

In a concise way QRST integral maps are characterized by the beat-to-beat sequence of NDI(intQRST), based on the c_i components of the KL expansion:

$$\mathrm{NDI(intQRST)} = \frac{\sum_{i=4}^{12} c_i^2}{\sum_{i=1}^{12} c_i^2} = \frac{P_{\mathrm{ND}}}{P_{\mathrm{D}} + P_{\mathrm{ND}}} \cdot 100\% \tag{4}$$

where P_D: BSPM signal power represented by the "dipolar" KL components (i: 1–3). P_{ND}: BSPM signal power represented by the "non-dipolar" KL components (i: 4–12) according to Lux et al. [6].

Two clinical examples to be interpreted by our conceptual heart and chest model are shown in Fig. 3. A brief summary of the data acquisition and processing is as follows. Unipolar ECG leads were recorded in supine rest position from 64 chest locations by the BioSemi Mark-8 system in accordance with the electrode layout suggested in Amsterdam. The length of the records was 5 min with the sampling rate of 2 kHz and the AD resolution of 24 bits. Data processing started with the identification of individual beats, Q_{on}, and T_{end} points were manually marked based on the "papillon-diagram" of superimposed leads. Ventricular ectopic beats and the subsequent beats were excluded from all the records. After a linear base-line adjustment from the measured 64 ECG signals, ECG signals were estimated in 128 unmeasured chest locations of the 192-lead regular measuring point setup introduced at the CVRTI, Salt Lake City. Finally, beat-to-beat QRST integral maps and NDI values were computed from the resultant dataset of the 192-lead system [11].

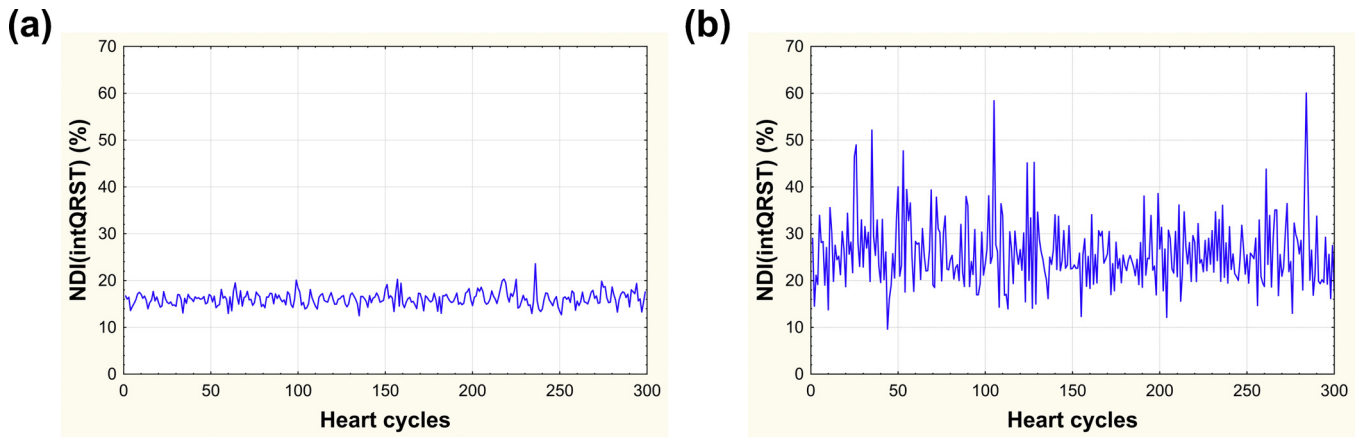

Fig. 3. Clinical measurement of a healthy subject (a) and an ICD patient (b). The graphs show the NDI values in 300 subsequent heart cycles. In the case of ICD patient ectopic beats and the subsequent beats were excluded, only the normal sine beats were analyzed. These clinical measurements were interpreted by the modelling examples shown in Fig. 4.

3. Results

Examples of our modelling results are summarized in a concise form in Fig. 4 utilizing the simplified APD profiles taken by Glukhov et al. [12]. His results provide modelling APD data for a normal subject and a FH patient. The data drawn after the real measurements characterize the mean value of the APD. SD data were borrowed from the study of Zaniboni et al. [13].

Derived from exactly the same model, Table 1 shows the results of the simplified dipolar approach of risk assessment following the method elaborated by Tereshchenko et al. [10,23]. In Table 1 we used modelling time and amplitude units (mtu and amu) instead of the physical units of the original papers. The comparison of NDI and SAI QRST values in Fig. 5(a) confirms the tendency of the SAI QRST in the down sloping range of transmural gradients. Furthermore, if we assume that the rows in Table 1 correspond to subsequent modelled heart cycles, the changes of the vectorcardiogram (VCG) parameters are visible in columns 5–7 and in Fig. 5(b).

4. Discussion

An early theoretical study of Lesh et al. [25] assumed and proved that by increasing the cell-to-cell coupling resistance of the myocardium, the dispersion of the APD should be more and more unmasked. The sophisticated experimental proof of this expectation was given later by Zaniboni et al. [13]. The first human measurement of APD distribution in healthy and failing heart was published by Glukhov et al. [12].

In this study our numerical heart model was used for the investigation of various MoAP properties compatible with the experimental findings of Glukhov et al., Zaniboni et al. and Pueyo et al. [12–14]. The macroscopic cell properties of healthy (H) and failing heart (FH) were approximated layer-by-layer for H and FH tissues. In both cases, transmural profiles were expressed in each layer by the mean value and the standard deviation of the APD. The mean value was constant throughout the subsequent modelled heart cycles, but the additive independent Gaussian noise was different beat-to-beat in accordance with the variability measurements of Zaniboni et al. and Pueyo et al. [13,14]. In other words, we assumed that in each modelled cardiac cycle the APD profile can be interpreted as a 5 dimensional random process (each dimension corresponds to one layer of the heart model) and the beat-to-beat profiles were possible realizations of the underlying random process. On cellular level the noise component was explained by the random $I(Ks)$ ionic fluctuations [13,14].

In the FH case (represented by profile B) in the subepicardial layers we supposed 2.5% as coefficient of variability ($CV = SD/APD_{90} \times 100\%$) due to the diminished gap-junctional

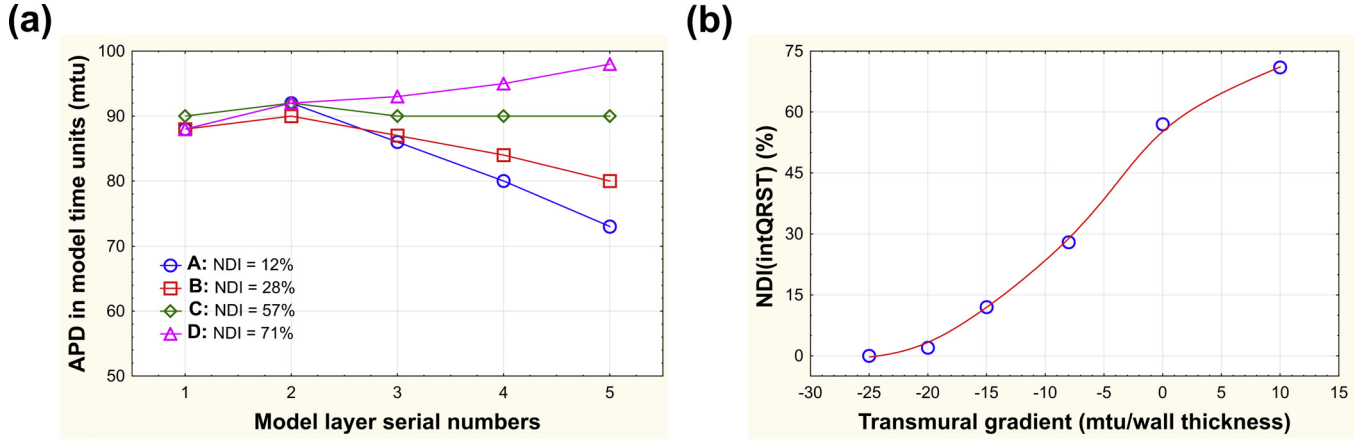

Fig. 4. (a) Transmural APD patterns. 'A' represents a normal subject and 'C' indicates the APD profile of a failing heart patient after Glukhov et al. [12]. 'B' and 'D' mark possible random realizations of APDs around profile C due to the diminished cell-to-cell coupling. The median and extreme NDI values are similar to the clinical example shown in Fig. 3. (b) NDI vs. transmural gradient graph estimated by our model.

Table 1
Simulated ECG parameters in the case of APD profiles A–D.

APD profiles	NDI (%)	Transmural gradient of APD (mtu)	SAI QRST × 10^5 (amu mtu)	SVG amplitude[a] × 10^5 (amu mtu)	SVG azimuth[a] (degrees)	SVG elevation[a] (degrees)
A	12	−15	216.653	93.503	41.2	44.9
B	28	−8	154.210	56.320	54.8	48.2
C	57	0	143.549	36.323	65.04	54.8
D	71	10	187.618	26.093	121.83	−16.9

[a] Definitions of spatial ventricular gradient (SVG) amplitude and SVG azimuth and elevation angles were taken from [23].

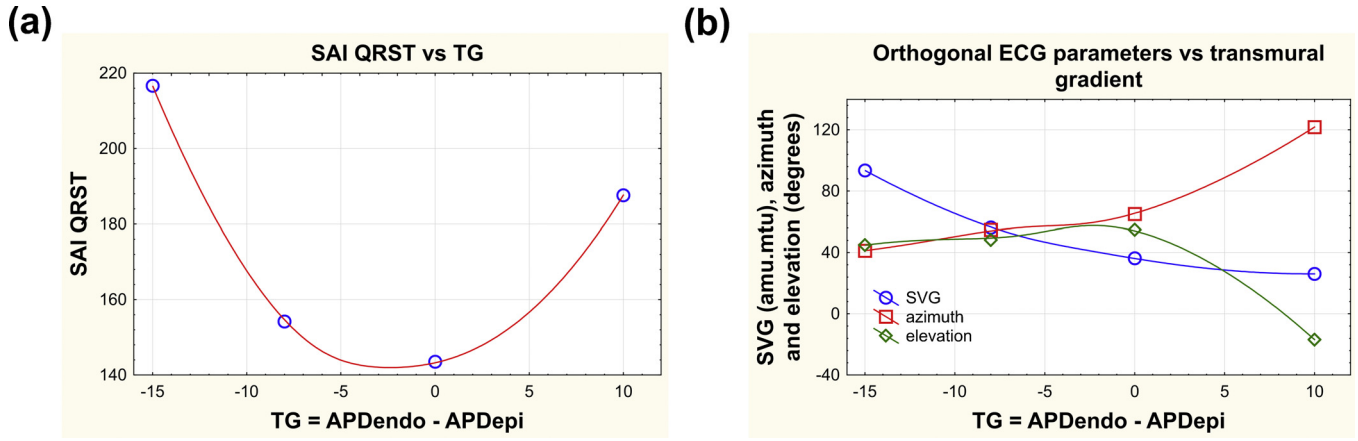

Fig. 5. (a) Simulated characteristics of the sum absolute QRST integral (SAI QRST) vs. the transmural gradients corresponding to the APD profiles shown in Table 1. (See [10,23] for the definition of SAI QRST.) (b) Simulated orthogonal ECG parameters vs. transmural gradients of the simulations corresponding to the APD profiles shown in Table 1. (SVG means spatial ventricular gradient, the definitions of the azimuth and elevation of SVG can be found in [23].)

coupling [13]. In Fig. 4(a) the extreme "mesoscopic" profiles represented by profiles A and C are "possible realizations". The corresponding NDIs were calculated according to Eq. (4) from the simulated QRST integral maps obtained by Eq. (3). The resultant NDIs are depicted in Fig. 4(b). Clearly, NDI values depend heavily on the beat-to-beat changing of APD profiles. In the example presented, the large amplitude NDI spikes were generated if the instantaneous APD realizations approached profile D in Fig. 4(a). Oppositely, a deviation towards the normal APD makes the NDI of profile B to converge to the normal profile of A (Fig. 4(a)).

In the healthy case the CV value was approximated as 1%. Due to the low initial NDIs (profile A) despite of the additive low amplitude noise, the frequent (within $M \pm 2SD$) NDI variations will be small, in complete accordance with the clinical measurements shown in Fig. 3(a). However, significant spikes in normal subjects are still possible, but very rare. This probabilistic nature explains that even in pathological case we may expect a few beats in the normal range of NDI (<20% according to Abildskov et al. [7]), and oppositely, even in the case of healthy subjects we may experience relatively high NDI spikes once in a while (Fig. 4(b)).

At this point we should refer to our previous modelling study, where APD profiles similar to that one studied now in the apical region were systematically applied to the mid-anterior, mid-lateral and mid-posterior regions. These modulations caused significant but low amplitude NDI spikes [15]. In similar experiments the use of epicardial QRST integral distributions instead of the body surface QRST integrals could reveal more accurately the locations of the irregularities of APD distribution. The reason of the information loss regarding the body surface distribution is related to the smoothing effect of the epicardial-to-body surface transfer This conclusion is supported by the findings of Burnes et al. [24], verifying by experimental examples that body surface potential distributions do not reflect the details of the patterns of epicardial integral maps.

Because NDI relates to dipolar and non-dipolar KL coefficients (according to Eq. (4)), on the very same experimental setup we have studied the SAI QRST method suggested by Tereshchenko et al. [10]. The modification of APD involves a change in NDI and TG as well. Table 1 and Fig. 5(a) depict the TG vs. SAI QRST relationship. We have to emphasize, that in our model studies we used model units in the voltage and also in the time domain, consequently our results are numerically directly not comparable with the experimental results found in [23]. However the tendencies comprised in Table 1 and Fig. 5 are comparable. We could verify that corresponding to a highly pathological mean APD profile (with low transmural APD gradient) a low SAI QRST value belonged [10], however the inversion of the transmural gradient vector (profiles) could enhance the SAI QRST value again. In these cases no beat-to-beat information was gained.

The possibility of beat-to-beat dynamic VCG measurements (in comparison of normal male and female population) was emphasized in [23]. In that comparison SAI QRST, spatial ventricular gradient (SVG), azimuth and elevation angles of SVG, and many other parameters were computed and statistically evaluated. In our model study using just a few dynamic VCG parameters we could demonstrate the utility of the parameters quoted above. In Fig. 5(b) the essential SVG parameters are depicted vs. the transmural gradient (TG) data. Assuming that TG data are changing from beat-to-beat, the graphs illustrate the range of expected VCG parameter changes due to the changes in the subsequent beats (APD profiles).

5. Conclusions

In this study, in a simplified but perfectly known environment we made an attempt to integrate recent cellular, tissue level and clinical observations, and estimate their clinical level consequences. Obviously the study due to the use of a simplified conceptual model could not explore the fine details of the spatio-temporal heterogeneity dynamics of the healthy and failing heart, still we think that we could get closer to the understanding of the

development of arrhythmia prone situation including its steady degradation (due to the slow degradation of APD mean profiles, denoted by B, C and D in our study).

According to our impression, the advantages of QRST integral map-based beat-to-beat heterogeneity measurements are as follows: (a) clear theoretical background, (b) potential possibility of the identification of the regional sources of the lability (by solving the relevant inverse problem), and (c) low noise sensitivity in the phase of measurements.

Acknowledgements

We acknowledge the financial support of the Hungarian State and the European Union under the programme TÁMOP-4.2.2.A-11/1/KONV-2012-0073 (Project title: "Telemedicine-focused research activities in the field of Mathematics, Informatics and Medical sciences"), of the Slovak Research and Development Agency under the programme APVV-0513-10 and of the VEGA Grant Agency, Slovakia under the programme 2/0131/13.

References

[1] J.J. Goldberger, M.E. Cain, S.H. Hohnloser, A.H. Kadish, B.P. Knight, M.S. Lauer, B.J. Maron, R.L. Page, R.S. Passman, D. Siscovick, W.G. Stevenson, D.P. Zipes, American Heart Association/American College of Cardiology Foundation/Heart Rhythm Society scientific statement on noninvasive risk stratification techniques for identifying patients at risk for sudden cardiac death: a scientific statement from the American Heart Association Council on Cardiology Committee on Electrocardiography and Arrhythmias and Council on Epidemiology and Prevention, Circulation 118 (2008) 1497–1518.

[2] J.A. Abildskov, L.S. Green, A.K. Evans, R.L. Lux, The QRST deflection area of electrograms during global alterations of ventricular repolarization, J. Electrocardiol. 15 (1982) 103–107.

[3] R. Plonsey, A contemporary view of the ventricular gradient of Wilson, J. Electrocardiol. 12 (1979) 337–341.

[4] D.B. Geselowitz, The ventricular gradient revisited: relation to the area under the action potential, IEEE Trans. Biomed. Eng. 30 (1983) 76–77.

[5] C.L. Hubley-Kozey, L.B. Mitchell, M.J. Gardner, J.W. Warren, C.J. Penney, E.R. Smith, B.M. Horácek, Spatial features in body-surface potential maps can identify patients with a history of sustained ventricular tachycardia, Circulation 92 (1995) 1825–1838.

[6] R.L. Lux, A.K. Evans, M.J. Burgess, R.F. Wyatt, J.A. Abildskov, Redundancy reduction for improved display and analysis of body surface potential maps. I. Spatial compression, Circulation 49 (1981) 186–196.

[7] J.A. Abildskov, L.S. Green, R.L. Lux, Detection of disparate ventricular repolarization by means of the body surface electrocardiogram, in: D.P. Zipes, J. Jalife (Eds.), Cardiac Electrophysiology and Arrhythmias, Grune & Stratton, New York, 1985, pp. 495–499.

[8] R.D. Berger, E.K. Kasper, K.L. Baughman, E. Marban, H. Calkins, G.F. Tomaselli, Beat-to-beat QT interval variability: novel evidence for repolarization lability in ischemic and nonischemic dilated cardiomyopathy, Circulation 96 (1997) 1557–1565.

[9] W.L. Atiga, H. Calkins, J.H. Lawrence, G.F. Tomaselli, J.M. Smith, R.D. Berger, Beat-to-beat repolarization lability identifies patients at risk for sudden cardiac death, J. Cardiovasc. Electrophysiol. 9 (1998) 899–908.

[10] L.G. Tereshchenko, A. Cheng, B.J. Fetics, B. Butcher, J.E. Marine, D.D. Spragg, S. Sinha, D. Dalal, H. Calkins, G.F. Tomaselli, R.D. Berger, A new electrocardiogram marker to identify patients at low risk for ventricular tachyarrhythmias: sum magnitude of the absolute QRST integral, J. Electrocardiol. 44 (2011) 208–216.

[11] G. Kozmann, K. Haraszti, I. Préda, Beat-to-beat interplay of heart rate, ventricular depolarization, and repolarization, J. Electrocardiol. 43 (2010) 15–24.

[12] A.V. Glukhov, V.V. Fedorov, Q. Lou, V.K. Ravikumar, P.W. Kalish, R.B. Schuessler, N. Moazami, I.R. Efimov, Transmural dispersion of repolarization in failing and nonfailing human ventricle, Circ. Res. 106 (2010) 981–991.

[13] M. Zaniboni, A.E. Pollard, L. Yang, K.W. Spitzer, Beat-to-beat repolarization variability in ventricular myocytes and its suppression by electrical coupling, Am. J. Physiol. Heart Circ. Physiol. 278 (2000) 677–687.

[14] E. Pueyo, A. Corrias, L. Virág, N. Jost, T. Szél, A. Varró, N. Szentandrássy, P.P. Nánási, K. Burrage, B. Rodríguez, A multiscale investigation of repolarization variability and its role in cardiac arrhythmogenesis, Biophys. J. 101 (2011) 2892–2902.

[15] G. Kozmann, G. Tuboly, Z. Tarjányi, V. Szathmáry, J. Švehlíková, M. Tyšler, Model interpretation of body surface potential QRST integral map variability in arrhythmia patients, Biomed. Signal Process. Control 12 (2014) 3–9.

[16] V. Szathmáry, R. Osvald, An interactive computer model of propagated activation with analytically defined geometry of ventricles, Comput. Biomed. Res. 27 (1994) 27–38.

[17] D. Durrer, R.T.H. Van Dam, G.E. Freud, M.J. Janse, F.L. Meijler, R.C. Arzbaecher, Total excitation of the isolated human heart, Circulation 41 (1970) 899–912.

[18] G.M. Hutchins, B.H. Bulkley, G.W. Moore, M.A. Piasio, F.T. Lohr, Shape of the human cardiac ventricles, Am. J. Cardiol. 41 (1978) 646–654.

[19] M.R. Franz, K. Bargheer, W. Rafflenbeul, A. Haverich, P.R. Lichtlen, Monophasic action potential mapping in human subjects with normal electrocardiograms: direct evidence for the genesis of the T wave, Circulation 75 (1987) 379–386.

[20] R.C. Barr, T.C. Pilkington, J.P. Boineau, M.S. Spach, Determining surface potentials from current dipoles, with application to electrocardiography, IEEE Trans. Biomed. Eng. 13 (1966) 88–92.

[21] M. Tyšler, M. Turzová, M. Tiňová, J. Švehlíková, E. Hebláková, V. Szathmáry, S. Filipová, Use of body surface potential maps for model-based assessment of local pathological changes in the heart, Bull. Pol. Acad. Sci.: Tech. Sci. 53 (2005) 207–215.

[22] M. Stenroos, The transfer matrix for epicardial potential in a piece-wise homogeneous thorax model: the boundary element formulation, Phys. Med. Biol. 54 (2009) 5443–5455.

[23] S. Sur, L. Han, L.G. Tereshchenko, Comparison of sum absolute QRST integral, and temporal variability in depolarization and repolarization, measured by dynamic vectorcardiography approach, in healthy men and women, PLoS ONE 8 (2013) e57175.

[24] J.E. Burnes, R.N. Ghanem, A.L. Waldo, Y. Rudy, Imaging dispersion of myocardial repolarization, I: comparison of body-surface and epicardial measures, Circulation 104 (2001) 1299–1305.

[25] M.D. Lesh, M. Pring, J.F. Spear, Cellular uncoupling can unmask dispersion of action potential duration in ventricular myocardium. A computer modeling study, Circ. Res. 65 (1989) 1426–1440.